remote sensing

MDPI

Article

Retrieval and Validation of Water Turbidity at Metre-Scale Using Pléiades Satellite Data: A Case Study in the Gironde Estuary

Yafei Luo [1,*], David Doxaran [2] and Quinten Vanhellemont [3]

[1] College of Electronic and Information Engineering, Guangdong Ocean University, Zhanjiang 524088, China
[2] Laboratoire d'Océanographie de Villefanche, UMR 7093 - CNRS/SU, 06230 Villefranche-sur-mer, France; david.doxaran@obs-vlfr.fr
[3] Royal Belgian Institute of Natural Sciences, Operational Directorate Natural Environments, 1000 Brussels, Belgium; qvanhellemont@naturalsciences.be
* Correspondence: luoyafei12@mails.ucas.ac.cn; Tel.: +86-0759-2396032

Received: 10 February 2020; Accepted: 12 March 2020; Published: 14 March 2020

Abstract: This study investigated the use of frequent metre-scale resolution Pléiades satellite imagery to monitor water quality parameters in the highly turbid Gironde Estuary (GE, SW France). Pléiades satellite data were processed and analyzed in two representative test sites of the GE: 1) the maximum turbidity zone and 2) the mouth of the estuary. The main objectives of this study were to: (i) validate the Dark Spectrum Fitting (DSF) atmospheric correction developed by Vanhellemont and Ruddick (2018) applied to Pléiades satellite data recorded over the GE; (ii) highlight the benefits of frequent metre-scale Pléiades observations in highly turbid estuaries by comparing them to previously validated satellite observations made at medium (250/300 m for MODIS, MERIS, OLCI data) and high (20/30 m for SPOT, OLI and MSI data) spatial resolutions. The results show that the DSF allows for an accurate retrieval of water turbidity by inversion of the water reflectance in the near-infrared (NIR) and red wavebands. The difference between Pléiades-derived turbidity and field measurements was proven to be in the order of 10%. To evaluate the spatial variability of water turbidity at metre scale, Pléiades data at 2 m resolution were resampled to 20 m and 250 m to simulate typical coarser resolution sensors. On average, the derived spatial variability in the GE is lower than or equal to 10% and 26%, respectively, in 20-m and 250-m aggregated pixels. Pléiades products not only show, in great detail, the turbidity features in the estuary and river plume, they also allow to map the turbidity inside ports and capture the complex spatial variations of turbidity along the shores of the estuary. Furthermore, the daily acquisition capabilities may provide additional advantages over other satellite constellations when monitoring highly dynamic estuarine systems.

Keywords: Pléiades satellite data; high resolution; remote sensing; water turbidity; Gironde Estuary

1. Introduction

Estuarine and coastal waters are sensitive areas under increasing influence from anthropogenic activities, potential discharge of nutrients and pollutants from agriculture and industries, dredging activities, ports and offshore constructions, and also extreme weather events (such as more intense rainfalls) which may significantly impact water turbidity dynamics [1]. Broad-scale water quality information is important for such areas as it allows for monitoring of the impact of these activities. Field measurements and remote sensing observations are complementary tools for monitoring such environments. Passive remote sensing radiometric techniques provide measurements in the visible, near-infrared (NIR) and infrared spectral regions now at high spatial and temporal resolutions

to retrieve key water quality parameters such as surface temperature, turbidity, concentrations of suspended particulate matter (SPM) and chlorophyll-a (Chl-a) [2–10].

Over the last two decades, medium- (~300 m) and high- (~30 m) spatial-resolution satellite data have been used to map SPM concentrations and/or turbidity in estuaries and coastal waters [11–15]. For example, in the highly turbid Gironde Estuary (GE, France), several studies have demonstrated the potential of satellite data such as Satellite Pour l'Observation de la Terre (SPOT)/SPOT4 (Take5) [16–18], Landsat-Enhanced Thematic Mapper Plus (ETM+) and Landsat8-Operational Land Imager (OLI) [17,19] but also MODerate resolution Imaging Spectroradiometer (MODIS) [20,21] to map concentration and seasonal dynamics of SPM. Recently, new satellite sensors with improved spectral, signal-to-noise and/or spatial resolutions such as Gaofen-1 (GF-1) [22,23], Sentinel2-MultiSpectral Instrument (MSI) [24–26] have offered new capabilities to study coastal and inland waters.

Increasing the spatial resolution from ~300 m (MODIS, MEdium Resolution Imaging Spectrometer (MERIS), Ocean and Land Color Instrument (OLCI)) to ~30 m (OLI, SPOT) or ~10 m (MSI) allows for remote sensing of SPM in small estuaries and nearshore zones, and allows for the monitoring of ports and dredging operations. Very high-spatial-resolution satellite sensors such as IKONOS or WorldView-2 and airborne portable remote imaging spectrometers have been already used to map water quality parameters [27–31]. However, there was no operational atmospheric correction processing for such data over coastal or inland waters.

The Pléiades constellation is composed of two satellites (Pléiades 1A and 1B) launched in 2011 and 2012. The spatial resolution is 2.8 m in multi-spectral mode, 0.7 m in the panchromatic band, and the pixel size is resampled to 2 m and 0.5 m [32]. The performance of Pléiades sensors improved compared to IKONOS and WorldView-2 in terms of spatial and temporal resolutions, as well as dynamic range (12 bits compared to 11 bits). Pléiades data can be recorded on-demand daily over a specific study area and can be corrected for atmospheric effects using the publicly available algorithm developed by Vanhellemont and Ruddick (2018) [33]. These characteristics give Pléiades the potential to operationally monitor SPM and turbidity dynamics in estuaries. Its capabilities are tested here in the GE, a macro-tidal system located in the south-west of France characterized by moderately to extremely turbid waters.

SPM in the GE has already been successfully monitored with SPOT (20 m), Landsat ETM+/OLI (30 m) and MODIS (250 m) satellite data [16–21]. The present study based on Pléiades satellite data represents one step further with observations recorded at 2 m spatial resolution. Moreover, the daily revisit associated to Pléiades data is a major advantage in order to observe and monitor small time-scale events such as tidal cycles, dredging activities, and peak floods [1,34]. The limited number of Pléiades spectral bands is not a disadvantage for the monitoring of turbidity and sediment transport as only green, red and NIR spectral bands are needed for the estimation of SPM in turbid waters [19]. The objectives of the present study were to (i) validate the Dark Spectrum Fitting (DSF) atmospheric correction (Vanhellemont and Ruddick, 2018) applied to Pléiades satellite data recorded over turbid estuarine waters and (ii) highlight the benefits of such very high spatial resolution for the monitoring of water turbidity dynamics in estuarine environments, including nearshore zones and ports.

2. Data and Methods

2.1. Study Area

The study area is the GE (Figure 1) situated in the south-west of France. It is a typical test site for the remote sensing of turbid waters, where SPM concentrations vary from ~1 to ~1000 g·m^{-3} within surface waters. Suspended sediments are the dominant factor affecting the water signal, with concentrations fluctuating mainly depending on the discharges of the Dordogne and Garonne Rivers and on tidal currents [20]. We selected two subsets from the estuary (Figure 1b). The first one (test site 1) (Figure 1a) is the central part of the estuary where the maximum turbidity zone (MTZ) is usually located. The Pauillac autonomous turbidity station is operated in this area. The other subset (test site

2) (Figure 1c) is located in the moderately turbid mouth area where the river plume extends during high river discharge conditions.

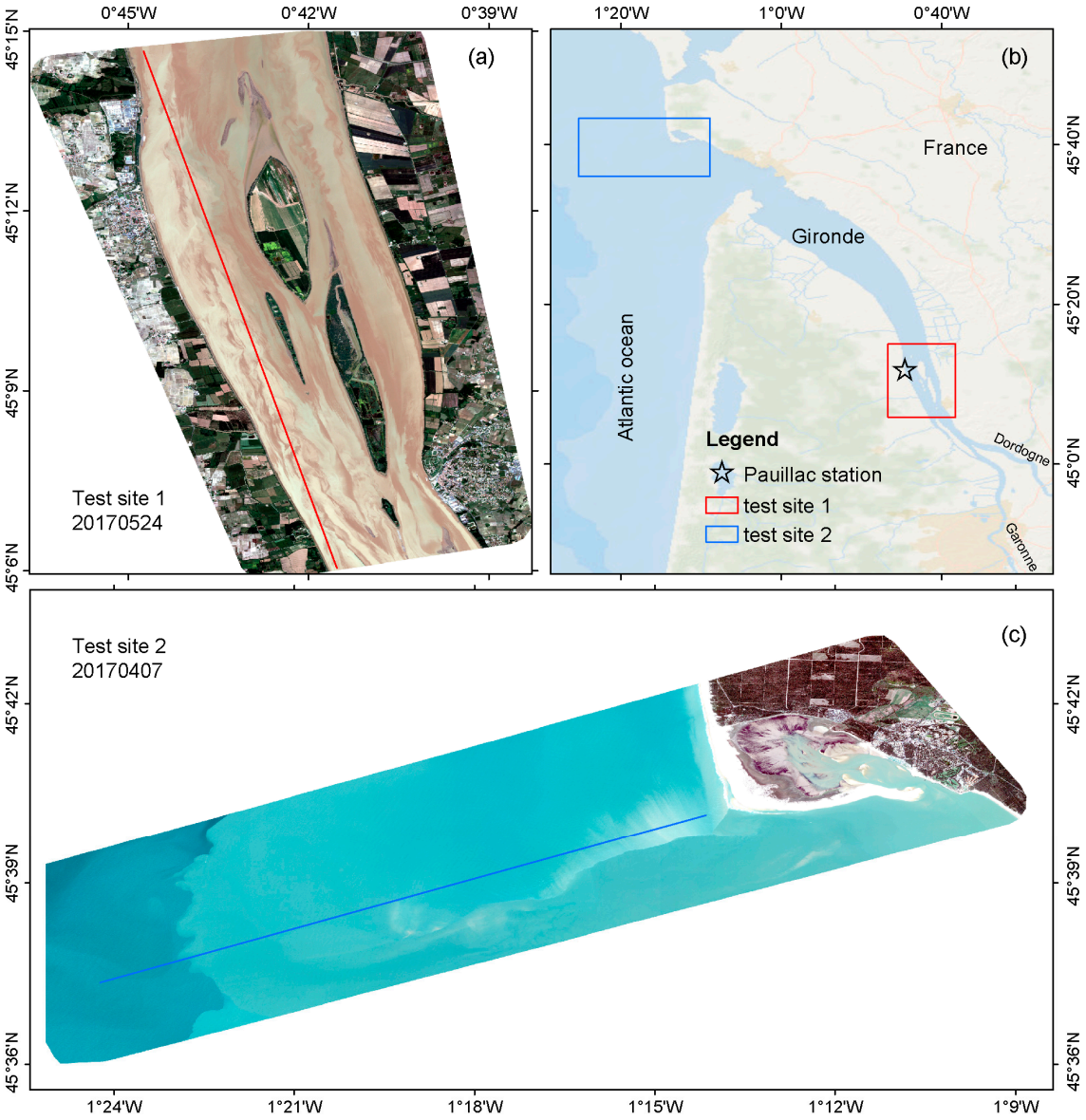

Figure 1. Study area: the Gironde Estuary (**a**–**c**). Locations of test site 1, test site 2 and Pauillac station (black star) (**b**). Pléiades quasi-true color images of the two test sites: test site 1 (**a**) and test site 2 (**c**). The red and blue lines in test sites 1 and 2 show the transects presented in Section 3.3.

2.2. Data Sets

2.2.1. Pléiades Imagery and DSF Atmospheric Correction

Table 1 presents and compares the specifications of Pléiades, SPOT-4, OLI and MODIS in terms of spatial, temporal and spectral resolutions. Twelve Pléiades images (Table 2) were recorded mainly from April to June 2017 over the GE: six images over the MTZ (test site 1), including one recorded in September 2018, and six images over the estuary mouth (test site 2). The full list of satellite images and corresponding tidal information is given in Table 2, as the tide may cause short timescale variability of SPM in the estuary.

Table 1. Specifications of Pléiades, Satellite Pour l'Observation de la Terre (SPOT-4), Landsat8-Operational Land Imager (OLI) and MODerate resolution Imaging Spectroradiometer (MODIS) satellite sensors.

Characters	Pléiades	SPOT-4	OLI	MODIS
Blue	450–520 nm	/	450–515 nm	459–479 nm
Green	520–600 nm	500–590 nm	525–600 nm	545–565 nm
Red	630–690 nm	610–680 nm	630–680 nm	620–670 nm
NIR	760–900 nm	780–890 nm	845–885 nm	841–876 nm
Spatial resolution	2 m	20 m	30 m	500/250 m
Revisit time	1–3 days	1–3 days	16 days	Daily

Table 2. Satellite data acquisition dates, times (Coordinated Universal Time, UTC), corresponding tidal conditions and satellite/sensor types. Tidal information is provided by the Service Hydrographique et Océanographique de la Marine (SHOM) in Pauillac and Cordouan, respectively, for test sites 1 and 2.

Test Sites	Image Date	Image Time	Time of High Tide	Tidal Range (m)	Satellite/Sensor
Test site 1	03/05/2017	11:15	10:57	3.7	Pléiades
Test site 1	24/05/2017	11:04	16:00	5.0	Pléiades
Test site 1	01/06/2017	10:52	10:24	3.6	Pléiades
Test site 1	10/06/2017	11:23	05:22	4.6	Pléiades
Test site 1	14/06/2017	10:52	07:38	3.9	Pléiades
Test site 1	19/09/2018	10:50	13:22	2.5	Pléiades
Test site 2	03/04/2017	10:56	08:48	3.1	Pléiades
Test site 2	06/04/2017	11:22	13:00	2.7	Pléiades
Test site 2	07/04/2017	11:15	13:57	3.0	Pléiades
Test site 2	19/04/2017	11:22	09:05	1.8	Pléiades
Test site 2	20/04/2017	11:15	11:01	1.7	Pléiades
Test site 2	21/04/2017	11:08	12:12	1.9	Pléiades
Test site 2	07/04/2017	10:53	13:57	3.0	Landsat8/OLI
Test site 2	07/04/2017	12:00	13:57	3.0	Terra/MODIS
Test site 2	07/04/2017	13:40	13:57	3.0	Aqua/MODIS

In order to retrieve water reflectance (the water reflectance used all along the study is the water-leaving reflectance, defined as $\rho = Rrs^{*}\pi$, dimensionless) and turbidity, the Dark Spectrum Fitting (DSF) atmospheric correction was applied, a method which maximises the strengths (spatial resolution) and minimises the weaknesses (spectral resolution) of Pléiades [33]. This method assumes negligible surface reflectance in at least one of the sensor bands, over the darkest pixel(s) in the image. Due to the typically small swath width of the sensors and hence the relatively limited spatial extent of the imagery, the path reflectance can be considered constant over an image or subscene. The atmospheric path reflectance was computed by using the radiative transfer model 6SV [35,36] for a number of aerosol models and for a number of bands, considering dark targets automatically detected in the scene. The best fitting aerosol model was then selected according to user defined criteria (e.g., the best fit to blue and NIR bands). In the present study, the model giving the lowest path reflectance was selected. Detailed information can be found in Vanhellemont and Ruddick (2018) [33].

2.2.2. Landsat/OLI and MODIS Satellite Data

Over test site 2 (mouth area), atmospherically corrected reflectances from Pléiades were compared to MODIS water reflectance values, used here as a reference to compensate for the lack of matchup with in situ data. MODIS/Terra and MODIS/Aqua images recorded on 7 April 2017 (Table 2) were corrected for atmospheric effects using the SeaDAS software [37], applying the NIR-SWIR atmospheric correction algorithm [38]. The time differences between Pléiades (11:15 UTC), MODIS/Terra (12:00 UTC) and MODIS/Aqua (13:40) data acquisitions on this day were 45 minutes and 2 hours 25 minutes, respectively.

The Pléiades water reflectances at 655 nm were compared to those retrieved from the 250 m MODIS band at 645 nm after spatial and spectral resampling. In the same way, Pléiades reflectance at 558 nm was compared to MODIS reflectance at 555 nm, with the original 500 m spatial resolution resampled to 250 m.

Moreover, Landsat8/OLI satellite data with a spatial resolution of 30 m for multispectral bands was used. On 7 April 2017, one Landsat8-OLI image was recorded over test site 2 at 10:53 UTC, i.e., only 22 minutes before the Pléiades image. OLI data were processed with the ACOLITE software selecting (for comparison) both the DSF and shortwave-infrared (SWIR) atmospheric correction methods [33,39] to retrieve water reflectance values.

2.2.3. In Situ Measurements

We first considered the autonomous in situ measurements recorded at the Pauillac station concurrently with Pléiades imagery. The Pauillac station is located along the western shore of the estuary by the port of Pauillac (Figure 2) and is part of the MAGEST network (http://magest.oasu.u-bordeaux.fr/), a high-frequency monitoring program of water quality [40,41]. Every 20 minutes, water temperature, salinity, and turbidity are measured at a 1-m depth, providing quasi-synchronous measurements with the Pléiades data. The two turbidity measurements recorded before and after Pléiades data acquisition times were linearly interpolated to the satellite overpass times.

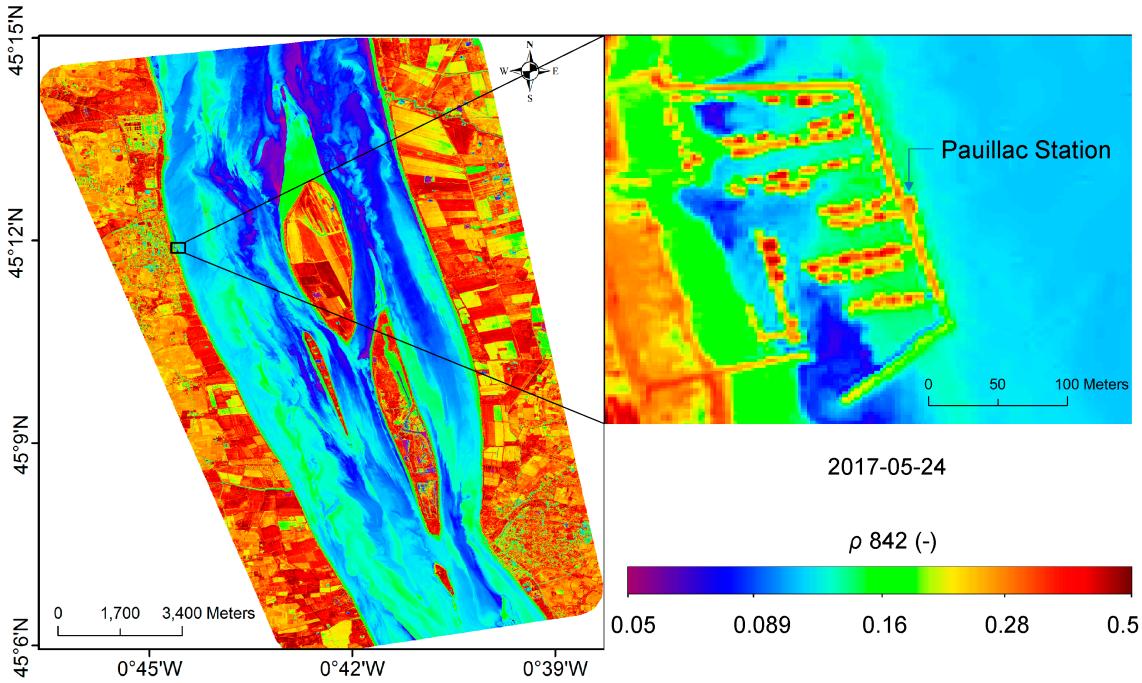

Figure 2. Pléiades-derived water reflectance at 842 nm (ρ842, dimensionless) recorded on 24 May 2017. The enlarged image locates the Pauillac autonomous station (0.742644 W, 45.198511 N).

The SeaSWIR 2013 dataset (simultaneous in situ measurements of water reflectance and turbidity at the Pauillac station [42,43]) was used for the calibration of the water turbidity algorithm and validation of Pléiades-retrieved water reflectances.

2.3. Methods

2.3.1. Calibration of Water Turbidity Algorithms

Based on the existing field measurements and knowledge in the Gironde Estuary, test sites 1 and 2 present two different water types: highly turbid in the MTZ with SPM concentrations ranging from

~50 to ~3000 g·m^{-3} within surface waters [16] and moderately turbid with SPM concentrations ranging from ~0 to ~60 g·m^{-3} [21], respectively, corresponding to different optical signatures (spectral water reflectance values). Moreover, according to Novoa et al. (2017), different spectral bands should be considered to establish robust relationships between SPM and the water reflectance: NIR band in test site 1 and red band in test site 2 [19].

In test site 1, in situ hyperspectral water reflectance from SeaSWIR 2013 campaign [42,43] was weighted by the relative spectral response (RSR) of each sensor to obtain equivalent water reflectance values in the green, red and NIR bands of Pléiades, OLI and MODIS satellites sensors. The central wavelengths of the selected bands are 558, 655 and 842 nm for Pléiades, 561, 655 and 865 nm for OLI, 555, 645 and 859 nm for MODIS. A second-order polynomial was established between turbidity measured in Nephelometric Turbidity Unit (NTU) and Pléiades reflectance at 842 nm (Equation (1)) for test site 1:

$$\text{Turbidity (NTU)} = 37661 \times \rho 842^2 + 1845 \times \rho 842 \ (R^2 = 0.78) \quad (1)$$

In test site 2, the water reflectance in the NIR band is less sensitive to variations of SPM concentrations below ~60 g·m^{-3} while the red band reflectance to turbidity relationship is linear [19,21]. A linear relationship between water reflectance in the red band and turbidity was hence used for test site 2, where SPM concentration is generally lower than ~60 g·m^{-3} [19,21]:

$$\text{Turbidity (NTU)} = 531.5 \times \rho 655/0.88 \ (R^2 = 0.89) \quad (2)$$

2.3.2. Validation of Atmospheric Correction

In this study, the DSF atmospheric correction method applied to Pléiades data recorded over the GE was validated by a step-by-step comparison with already-validated satellite products and field measurements. For that purpose, Pléiades products were compared to (i) spectral relationships obtained from previous field measurements (see Section 3.1), (ii) already-validated satellite products (Section 3.1) and (iii) simultaneous field measurements of turbidity (Section 3.2).

Water reflectances from Pléiades were compared with same-day imagery from Landsat8-OLI and MODIS-Aqua/Terra recorded over a specific test site. Cloud-free satellite images were collected on 7 April 2017 within a ± 3 h time window, and imagery from the different sensors was reprojected onto the same grid, by resampling Pléiades data to a 30 m and 250 m spatial resolutions, using mean averaging. The green, red, and NIR reflectances from the different sensors were spectrally adjusted to the Pléiades spectral bands. In situ hyperspectral water reflectance measurements made in the GE in 2012 and 2013 [42,43] and the relative spectral responses (RSRs) of Pléiades-1B, OLI, MODIS-Aqua and MODIS-Terra sensors were used for this adjustment (Figure 3). The reflectance in the considered satellite spectral band was computed as

$$\rho_s = \int_{\lambda 1}^{\lambda 2} \rho_\lambda \times RSR(\lambda) d\lambda \Big/ \int_{\lambda 1}^{\lambda 2} RSR(\lambda) d\lambda \quad (3)$$

where ρ_s is the band specific reflectance, ρ_λ is the hyperspectral water reflectance in the GE, λ_1-λ_2 are the wavelengths defining the spectral range.

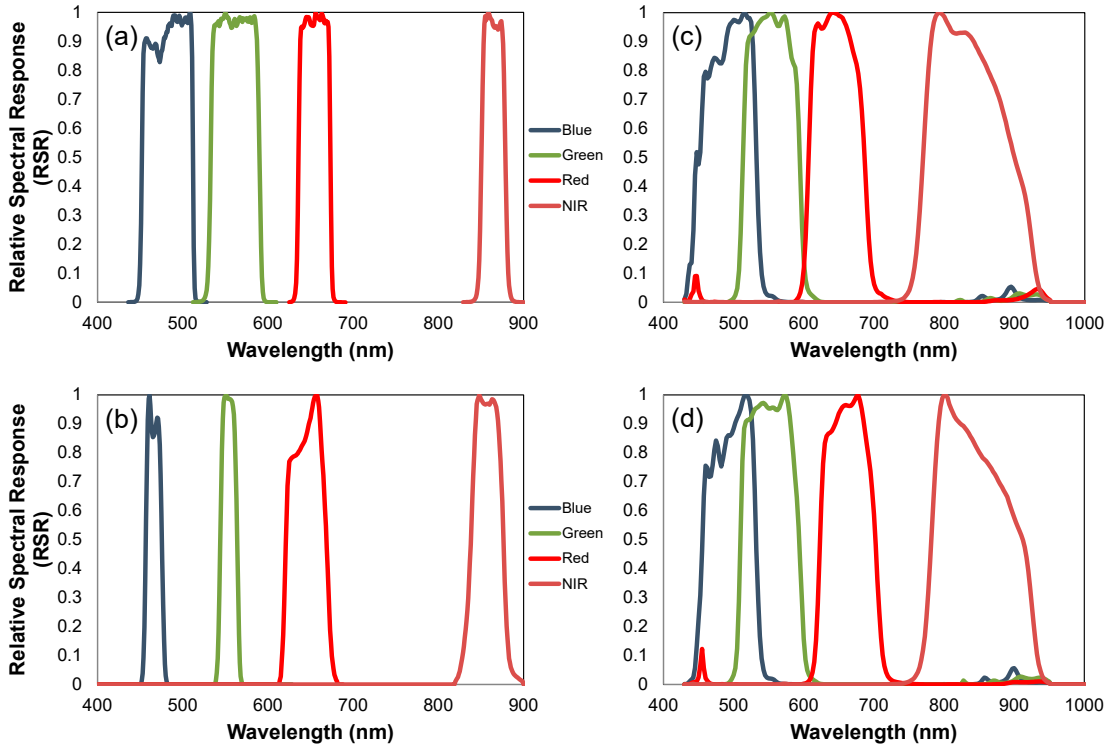

Figure 3. Relative Spectral Responses of OLI (**a**), MODIS (same for Terra and Aqua) (**b**), Pleiades-1A (**c**) and Pléiades-1B (**d**) at Blue, Green, Red and NIR wavebands.

Linear relationships were established between the water reflectance in OLI and MODIS bands and in the corresponding Pléiades band (Table 3).

Table 3. Relationships between water reflectance in the green, red and NIR spectral bands of Pléiades-1B and OLI and Pléiades-1B and MODIS sensors, where x is the water reflectance of OLI or MODIS as a function of y (water reflectance of Pléiades-1B).

Sensor	OLI to Pléiades			MODIS to Pléiades		
Band	**Relationships**	**RMSE**	**MAPE**	**Relationships**	**RMSE**	**MAPE**
Green	y = 0.94*x − 0.0005	0.0094	7%	y = 0.97*x + 0.0007	0.0040	3%
Red	y = 1.00*x − 0.0048	0.0027	1.5%	y = 1.00*x − 0.0080	0.0031	1.6%
NIR	y = 1.00*x + 0.0110	0.0123	18%	y = 0.99*x + 0.0092	0.0087	12%

Pléiades-derived turbidity values in the 2 × 5 pixel box around the Pauillac autonomous station were compared to simultaneous in situ measurements.

2.3.3. Downscaling of Pléiades Spatial Resolution

The usefulness of the very high spatial resolution of Pléiades for turbidity monitoring in the GE was examined by resampling the imagery. Original resolution products were compared to 20 m (e.g., SPOT or Sentinel-2/MSI) and 250 m (e.g., MODIS) products simulated by mean averaging.

Comparisons were made around the Pauillac autonomous station, along transects shown as red line in Figure 1b for test site 1 and as blue line in Figure 1c for test site 2 (see Section 3.4). Scatterplots comparing original and downscaled Pléiades data and comparative maps are shown in Section 3.4.

2.3.4. Accuracy Assessment

The Root Mean Square Error (RMSE) and Mean Absolute Percentage Error (MAPE) were used to quantitatively compare the water reflectance or turbidity values derived from different satellite data:

$$\mathrm{RMSE} = \sqrt{\frac{\sum_{i=1}^{n} (x_i - y_i)^2}{n}}, \tag{4}$$

$$\mathrm{MAPE} = \frac{\sum_{i=1}^{n} \left| (x_i - y_i)/y_i \right|}{n} \times 100\%, \tag{5}$$

where x_i and y_i are respectively the estimated reflectance or turbidity and reference reflectance or turbidity (in situ measurements or already-validated satellite products), n is the total number of samples.

The difference (Diff) between satellite-derived and field-measured turbidity values was computed to assess the validity of the satellite product as

$$\mathrm{Diff.} = \frac{(x_i - y_i)}{y_i} \times 100\%, \tag{6}$$

where x_i is the turbidity retrieved from satellite data and y_i is the turbidity measured in situ (Pauillac autonomous station).

3. Results

3.1. Validation of Pléiades-Retrieved Water Reflectances

According to the atmospheric corrections applied, the water reflectance values retrieved from Pléiades imagery (rhos) in the MTZ (test site 1) contribute up to 57% of the signal recorded at the top of the atmosphere (rhot) in the blue band; this contribution progressively increases in the green and red bands and reaches 89% in the NIR band (Figure 4a). The contribution of rhos to rhot is significantly lower in the moderately turbid waters in the estuary mouth (test site 2), varying from 16% in the NIR to ~50% in the blue and green bands (Figure 4b). This indicates that the top of atmosphere signal recorded over the turbid part of the estuary largely consists of the water signal while in the less turbid waters (test site 2), the water contribution is significantly lower. Higher uncertainties may be introduced in the turbidity product in clearer waters due to the higher relative contribution of atmospheric correction errors.

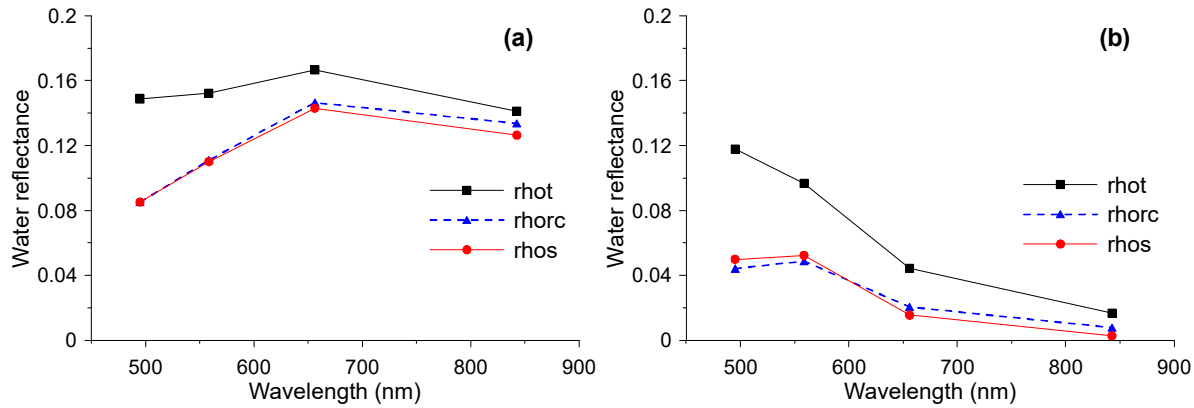

Figure 4. Examples of Pléiades-derived reflectance signal at the top of atmosphere (rhot), Rayleigh corrected reflectance (rhorc) and surface reflectance (rhos) after ACOLITE-DSF processing for (**a**) test site 1 on 24 May 2017, and (**b**) test site 2 on 7 April 2017.

The relationships between the Pléiades-derived water reflectance, respectively at 495, 558, 655 and 842 nm, and synchronous in situ turbidity values measured at the Pauillac autonomous station were compared to the relationships previously established based on in situ data (SeaSWIR dataset) for test site 1. The relationships retrieved from Pléiades data were comparable to those obtained from the field dataset (Figure 5). The in situ (blue points) and satellite (red points) water reflectance values vs. turbidity values overlap at 495 and 558 nm bands. The Pléiades-derived water reflectance signal at these two wavelengths tends to saturate in the highly turbid waters of the GE [44]. The ρ495 signal is apparently not sensitive to turbidity variations, and the same was observed at 558 nm. The saturation reflectance can be determined by a Nechad-type function [44,45], and was found to be 0.087 at 495 nm and 0.116 at 558 nm. The saturation effect had similar values of 0.081 and 0.123 in the in situ data. At higher turbidities of around 500 NTU, the Pléiades-derived water reflectance in the red band also saturates (0.160), again close to the in situ observation (about 0.164). The Pléiades-derived water reflectance at 865 nm shows a logarithmic increase with increasing turbidity without saturation, also as previously observed based on in situ measurements.

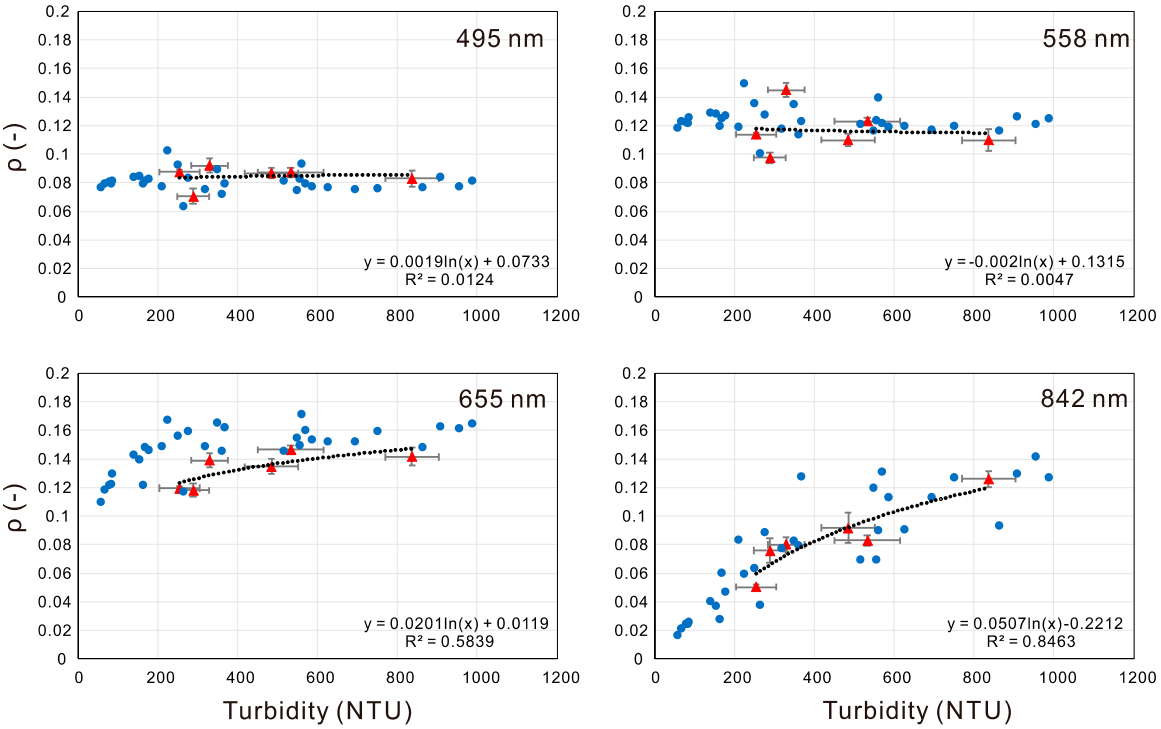

Figure 5. The red triangles the present relationships between Pléiades-derived water reflectance, respectively at 495, 558, 655 and 842 nm, and synchronous in situ turbidity values measured at the Pauillac autonomous station in 2017. The black dashed lines are the logarithmic relationships. The vertical bars show the standard deviation of the water reflectance values derived from Pléiades data over the ten pixels closest to the Pauillac field station. The horizontal bars show half the turbidity range between the two in situ measurements bounding the satellite overpass (i.e., their standard deviation). The blue points represent the relationships between the water reflectance and turbidity established using the in situ measurements (SeaSWIR dataset).

An indirect validation of the atmospheric correction is obtained by retrieval of similar spectral relationships (i.e., saturation reflectances) from in situ and satellite data and hence, the atmospheric correction yields satisfactory results for turbidity retrieval in the MTZ area where the water signal dominated at the top of the atmosphere.

Pléiades-derived green and red reflectances are then plotted as function of the corresponding OLI (Figure 6) and MODIS (Figure 7) water reflectances over test site 2 (data recorded on 7 April 2017).

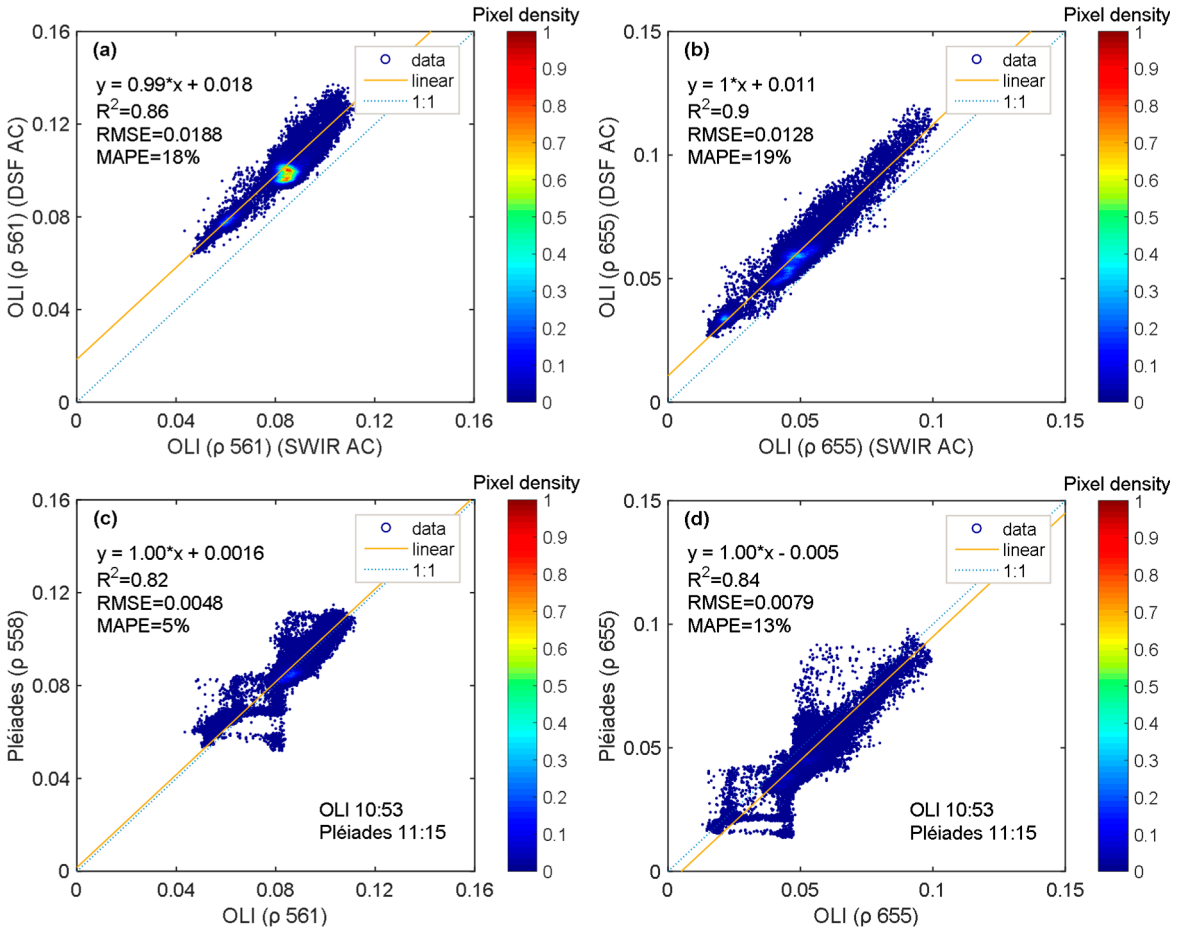

Figure 6. Comparisons between SWIR and DSF derived water reflectance values for OLI (ρ561) (**a**) and OLI (ρ655) (**b**). Comparisons between OLI (ρ561) and Pléiades (ρ558) (**c**), OLI (ρ655) and Pléiades (ρ655) (**d**) reflectance values over test site 2 on 7 April 2017.

OLI data were processed using ACOLITE using both DSF and SWIR atmospheric correction methods [33,39], which both showed a good correspondence to the Pléiades-retrieved reflectances (Figure 6a,b) with R^2 of ~0.9 and slope of ~1.00. SWIR-derived water reflectances were slightly lower than the DSF-derived ones, with intercepts of 0.018 and 0.011, in the green and red bands. The SWIR atmospheric correction was finally selected for OLI data processing as it provides the best agreement with Pléiades.

Pléiades and OLI water reflectances show good agreement (Figure 6c,d): the linear regression slopes are 1.00 for both the green (ρ561/ρ558) and red (ρ655/ρ655) bands with small intercepts, 0.0016 and -0.005. R^2 values are 0.82 and 0.84, with RMSE of 0.0048 and 0.0079 with MAPE of 5% and 13%.

Water reflectance values derived from Pléiades, MODIS/Terra and MODIS/Aqua were also compared over test site 2 (Figure 7). Two clusters are found in the scatter plots, which correspond to the turbid river plume (higher reflectances) and the clearer oceanic waters (lower reflectances). MODIS/Terra and Aqua products show some difference (MAPE ≤ 14%) due to the time difference between data acquisition (Figure 7a,b). Water reflectance values from MODIS and Pléiades data show a good agreement with linear regression slopes of the best-fitted linear relationships close to 1 in the red band, and slightly higher than 1 in the green band, with no significant intercept in either band. The corresponding MAPE is less than 16% (red) and less than 23% (green). This correspondence is reasonable due to the resolution and overpass time differences of the satellites.

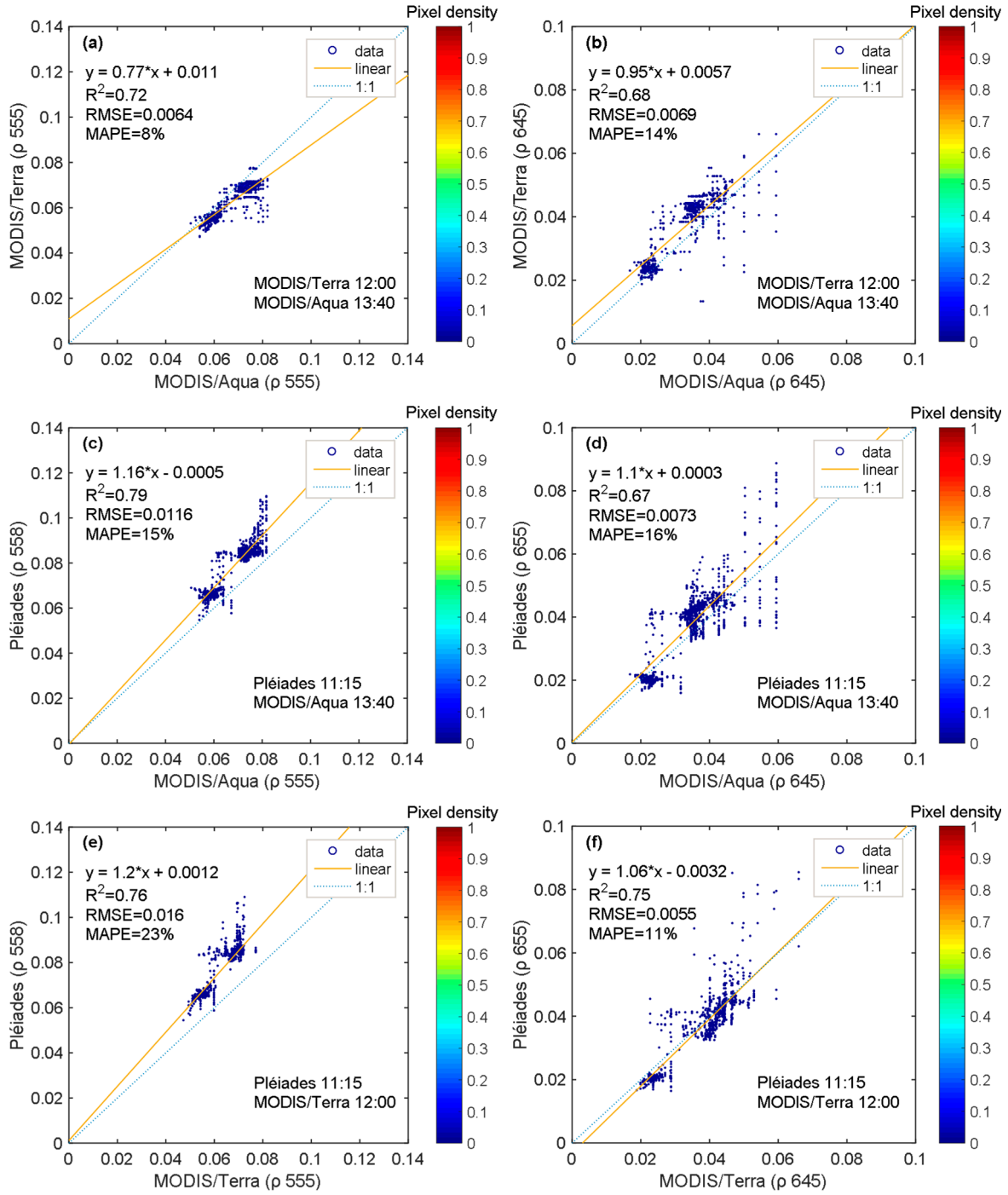

Figure 7. Comparisons between MODIS/Terra (ρ555) and MODIS/Aqua (ρ555) (**a**), MODIS/Terra (ρ645) and MODIS/Aqua (ρ645) (**b**), MODIS/Aqua (ρ555) and Pléiades (ρ558) (**c**), MODIS/Aqua (ρ645) and Pléiades (ρ655) (**d**), MODIS/Terra (ρ555) and Pléiades (ρ558) (**e**), and MODIS/Terra (ρ645) and Pléiades (ρ655) (**f**) water reflectance values (test site 2) on 7 April 2017.

3.2. Validation of Pléiades-Retrieved Water Turbidity

Turbidity was computed from Pléiades data using the NIR band reflectance for test site 1, and 6 matchups with the Pauillac station were identified (3 May 2017, 24 May 2017, 1 June 2017, 10 June 2017, 14 June 2017 and 19 September 2018).

Very good agreement between satellite and in situ turbidity was found for the range of 200–840 NTU (Figure 8b): RMSE of 43 NTU and MAPE of 10%. The linear regression slope is 0.99 and R^2 is

0.95. These results show a large improvement over using top-of-atmosphere (MAPE 57%) (Figure 8e) or Rayleigh-corrected (MAPE 40%) (Figure 8f) reflectances, indicating the need for a full atmospheric correction even for extremely turbid waters.

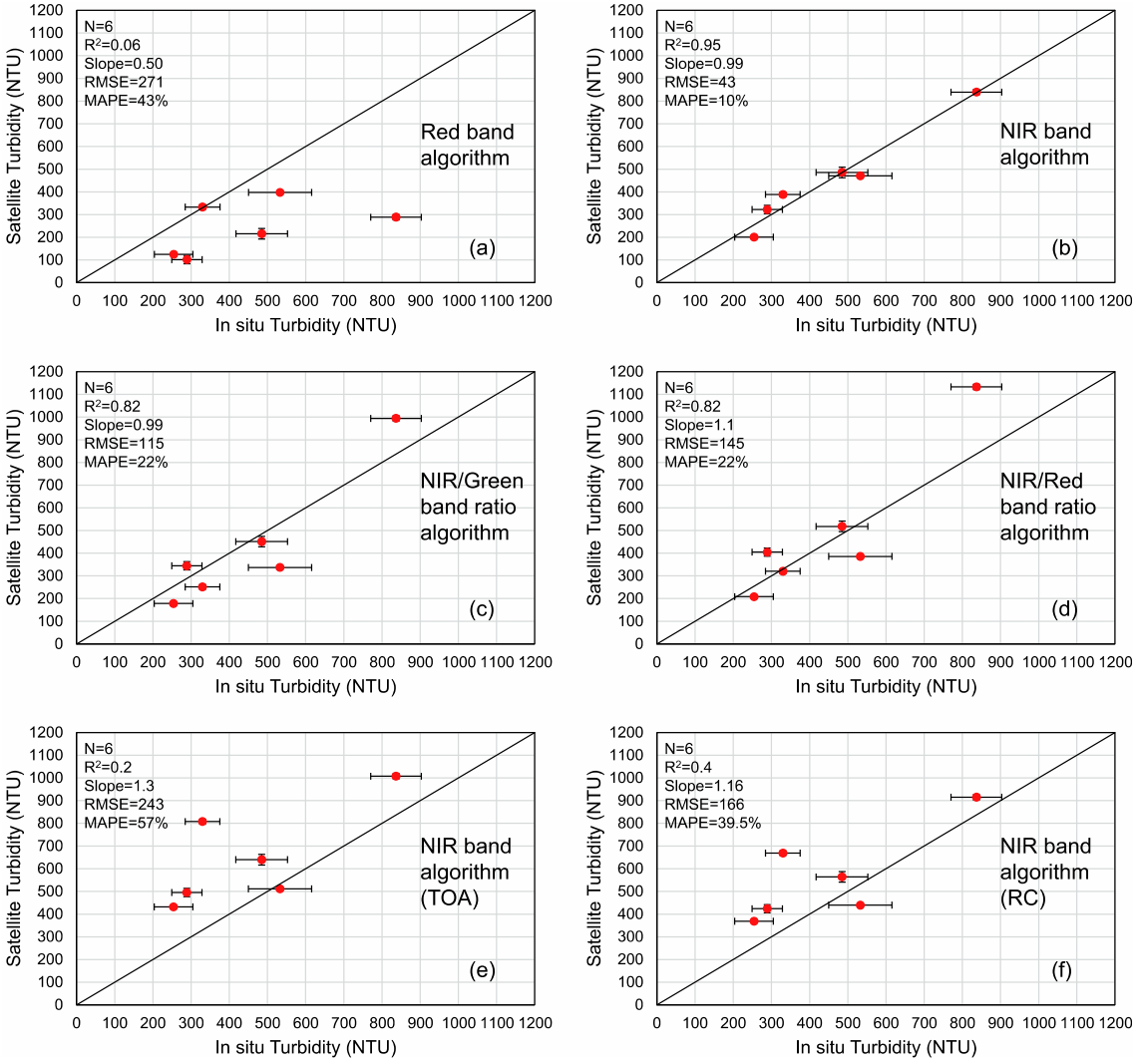

Figure 8. Pléiades-derived turbidity in Nephelometric Turbidity Unit (NTU) as function of in situ measured turbidity in the Pauillac autonomous station when using red band (**a**), NIR band (**b**), NIR/Green band ratio (**c**) and NIR/Red band ratio (**d**) algorithms. Same comparisons when using the top of atmosphere (TOA) reflectance in the NIR band (**e**) and Rayleigh-corrected (RC) reflectance in the NIR band (**f**). The vertical error bars show the standard deviation within the selected ten Pléiades pixels (±3 to ±23 NTU) and the horizontal error bars show half the range of the bounding in situ turbidity measurements (from ±40 to ±83 NTU).

Turbidity retrieved using red band or band ratio algorithms with best-fitted exponential relationships show less agreement with in situ turbidity. Much lower turbidity values are obtained using the red band algorithm due to the saturation of the water reflectance signal in this spectral region (Figure 8a, Figure 5). The saturation of water reflectance is even more obvious for the green band (Figure 5), the use of which would also result in the underestimation of water turbidity. The NIR/Green and NIR/Red band ratio algorithms (Figure 8c,d) show better results than single red or green bands, with MAPE of 22%. This proves that an NIR spectral band is required to estimate SPM concentrations (or turbidity) over the wide range of SPM concentrations encountered in the GE (10 to > 1000 g·m^{-3}) [16,19].

The temporal variability in the Pauillac site is larger than the instantaneous spatial variability around the site: compare the vertical (spatial variability) and horizontal (temporal variability) error bars in Figure 8.

3.3. Impact of Pléiades Band Designations on Water Reflectance and Turbidity Retrievals

3.3.1. Sensor-to-Sensor Band Differences Based on the Relative Spectral Responses

Compared to OLI and MODIS, the specifications of Pléiades bands do affect the water reflectance and turbidity retrievals. The Pléiades sensor has three visible and one NIR spectral bands and no SWIR band, so that only OLI and MODIS data can be corrected for atmospheric effects using the SWIR or NIR-SWIR algorithms.

The next step was to determine how the designation of Pléiades, OLI and MODIS bands (bandwidth, spectral resolution) affects the relationship between the water reflectance (ρ, dimensionless) and water turbidity (NTU) in the Gironde Estuary. For that, the relationships between the water reflectance values in the respective Green, Red and NIR spectral bands of these sensors were established, considering the differences in terms of spectral band sensitivity and widths. The field hyperspectral water reflectance measurements carried out in the Gironde Estuary in 2012 and 2013 [43] and the relative spectral responses (RSRs) (Figure 3) of Pléiades-1B, OLI and MODIS-A sensors were used in this purpose. The obtained relationships between the Green, Red and NIR spectral bands show that Pléiades reflectance match well with the corresponding OLI and MODIS bands, with simple linear relationships having a slope close to 1 and almost negligible intercepts in the Red and Green spectral bands (Figure 9, Table 3). By opposition a significant offset is systematically obtained in the NIR. The root mean square error (RMSE) is the minimum for the Green and Red bands (less than 0.010) and slightly higher in the NIR (~0.012). The mean absolute percentage error (MAPE) is systematically less than 7% in the Green and Red bands and up to 18% in the NIR.

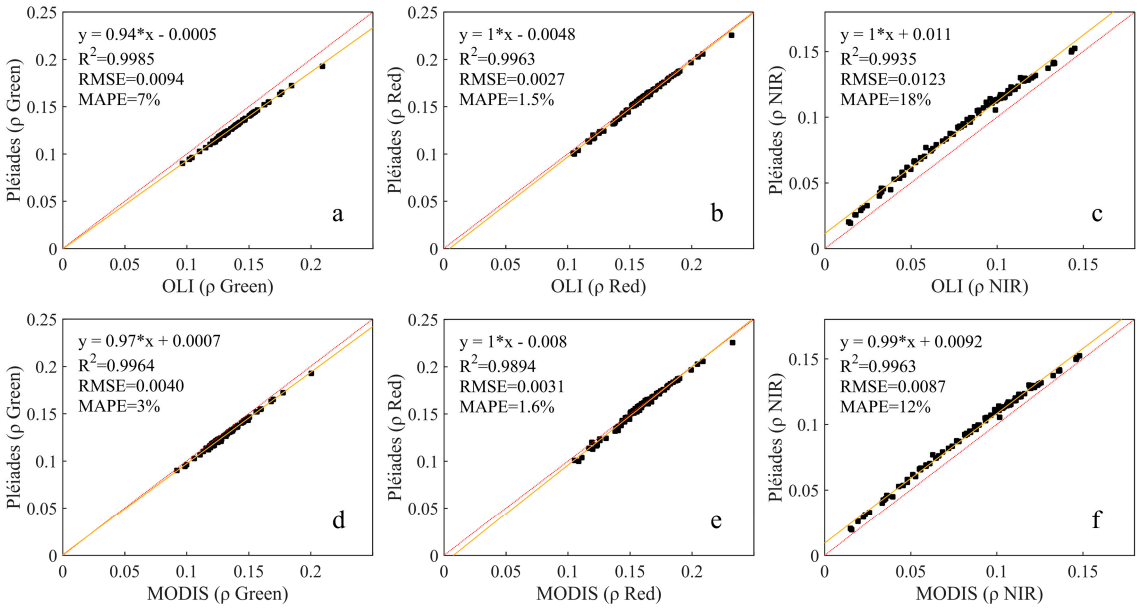

Figure 9. Relationships between water reflectance in the green, red and NIR spectral bands of Pléiades-1B and L8-OLI sensors (**a**–**c**), Pléiades-1B and MODIS-A (**d**–**f**). The red dashed lines are 1:1 lines and the oranges lines are the best Ordinary Least Squares linear fits.

In Green and Red bands, the reflectance sensed by Pléiades is slightly lower than that of MODIS and OLI. The lowest difference is observed between the OLI and Pléiades Red bands (1.5%). In the NIR band, the Pléiades water reflectance is a bit larger than that of MODIS and OLI. The bandwidth of

Pléiades is overall larger than OLI and MODIS, especially in the NIR band (Figures 3 and 9), where MAPE starts to become significant (12–18%), so sensor specific calibrations are needed (see Figure 10 and Table 4 below).

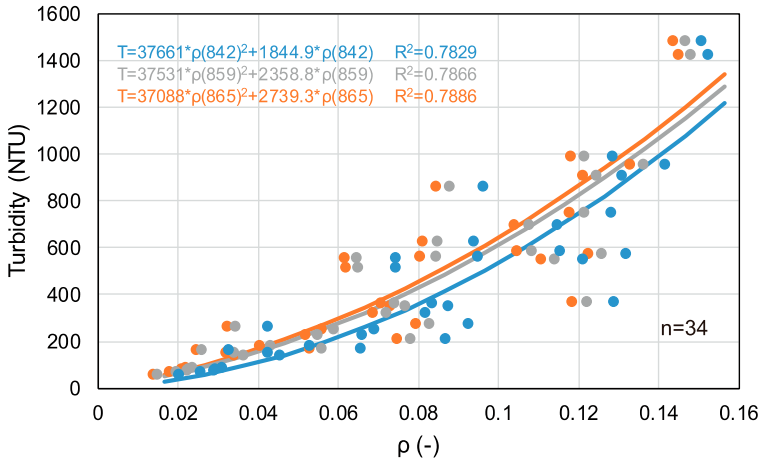

Figure 10. Empirical relationships established for test site 1 based on field measurements (2013 SeaSWIR survey) between water turbidity (NTU) and water reflectance in the NIR bands of Pléiades-1B (blue), OLI (red) and MODIS (grey).

Table 4. Validation results for Pléiades, OLI and MODIS turbidity algorithms.

Test Site 1	MAPE (%)	RMSE (NTU)
Pléiades	16.6%	107
OLI	15.0%	104
MODIS	15.4%	105

3.3.2. In Situ Water Reflectance and Turbidity Algorithms for Pléiades, OLI and MODIS

A polynomial relationship can provide satisfactory results in the maximum turbidity zone of the GE [19]. This relationship was tested on the SeaSWIR 2013 dataset (turbidity values ranging from 57.9 to 1484.7 NTU) (Figure 10). It provides good results with R^2 of 0.78 (N = 34) and the extra validation dataset (SeaSWIR 2012 turbidity and water reflectance measurements) (N = 16) (Table 4) showed MAPE values of 16.6%, 15.0%, 15.4%, respectively for Pléiades, OLI and MODIS. The three algorithms show similar patterns but still with some scatter. This is due to the NIR band spectral differences among the three sensors (Figure 9). The validation results show that the difference is lower for OLI sensor than MODIS and Pléiades. This probably results from the narrow bandwidth of OLI compared to the wider spectral range of Pléiades which may introduce more uncertainty.

3.4. Impact of Satellite Data Spatial Resolution on Turbidity Retrieval

Spatial variability was also examined using resampled Pléiades imagery by comparing the original 2 m data to simulated 20 and 250 m data. The effects of spatial resolution on the correspondence with in situ measurements at the Pauillac station on 24 May 2017 show differences of 0.31% for the 2 m, 8.27% for the 20 m and 26% for the 250 m resampled Pléiades imagery. The coarser resolution shows a worst correspondence with the in situ measurements due to the increase of turbidity to the shallow shores of the estuary, and mixed pixel effects that include land and platform reflectances (Figure 11).

Transects (indicated on Figure 1) of turbidity were compared at the different resolutions. Figure 12 shows the transect along the main navigation channel in test site 1 with a strong variability of turbidity. At the original resolution, the variability is sharp and complex, following the mud banks and turbulent currents, as previously observed using SPOT data [17]. At 20 and 250 m, the transect was smoothed, only preserving the main turbidity features. Good agreement between 2 m and 20 m data was found

(MAPE 2.5%), while a much larger difference was found for the comparison between 2 and 250 m data (MAPE 10%).

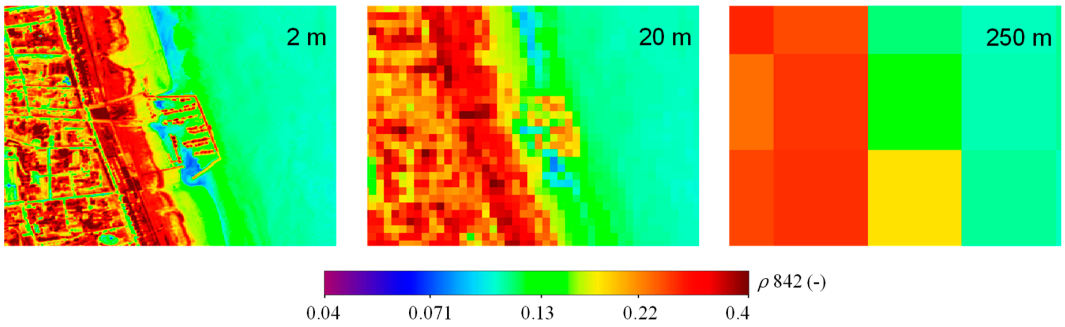

Figure 11. The Pauillac station area of Pléiades (2 m), 20 m and 250 m satellite images (24 May 2017).

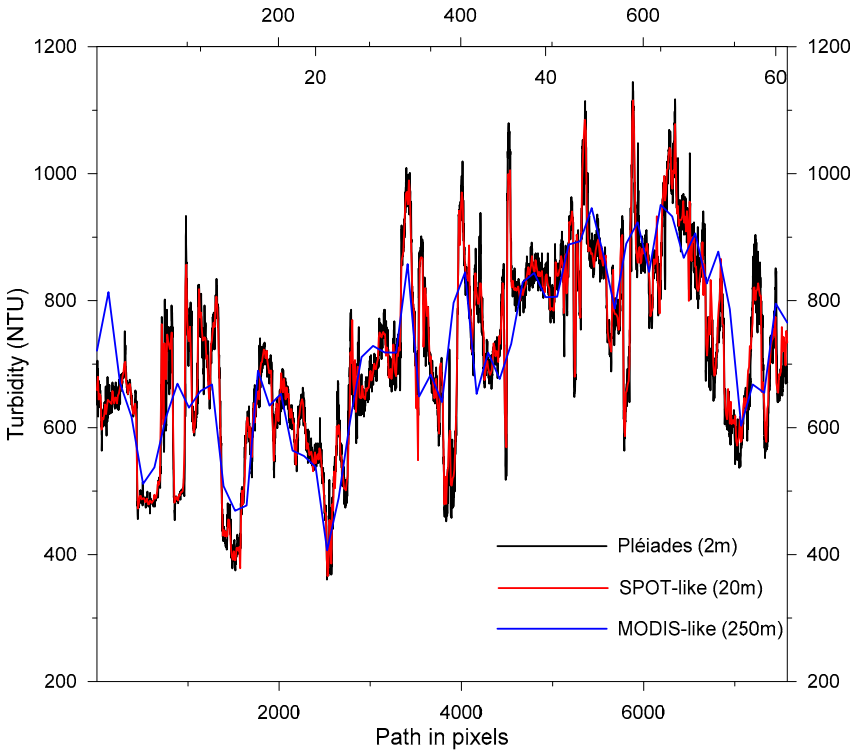

Figure 12. Comparisons between turbidity in Nephelometric Turbidity Unit (NTU) retrieved from Pléiades data at different spatial resolutions along a transect, from north to south in test site 1 (red line on Figure 1a) on 24 May 2017.

The transect for test site 2 (Figure 13) shows small-scale variability at 2 m data, but overall, the patterns are well preserved in the 20 and 250 m resampled data, showing low differences (MAPE of 2.8% and 4.1%, respectively).

The turbidity products at 2, 20 and 250 m were compared over the full study site; example maps are shown in Figure 14 for site 1 and Figure 15 for site 2. In site 1, the turbidity features are very well captured at both 2 and 20 m, but at 250 m only the main features remain. Mixed pixels along the shores and islands contaminate the product. The MAPE are 7.8% and 18%, respectively, for the 20 and 250 m products compared to the original 2 m data. The MAPE between the 20 and 250 m products is 13%. In the MTZ (site 1), a 20 m spatial resolution seems well adapted to map most turbidity features.

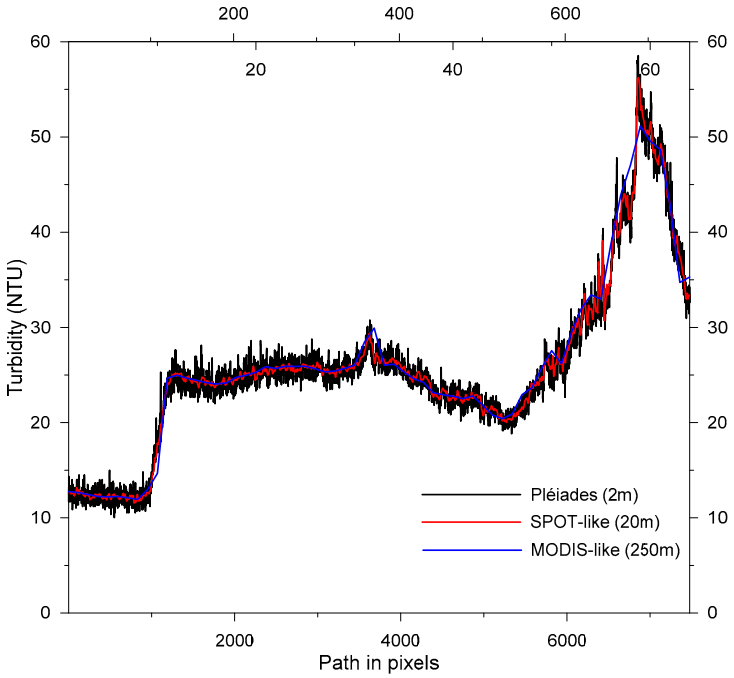

Figure 13. Comparisons between turbidity in Nephelometric Turbidity Unit (NTU) retrieved from Pléiades data at different spatial resolutions along a transect, from west to east in test site 2 (blue line on Figure 1c) on 7 April 2017.

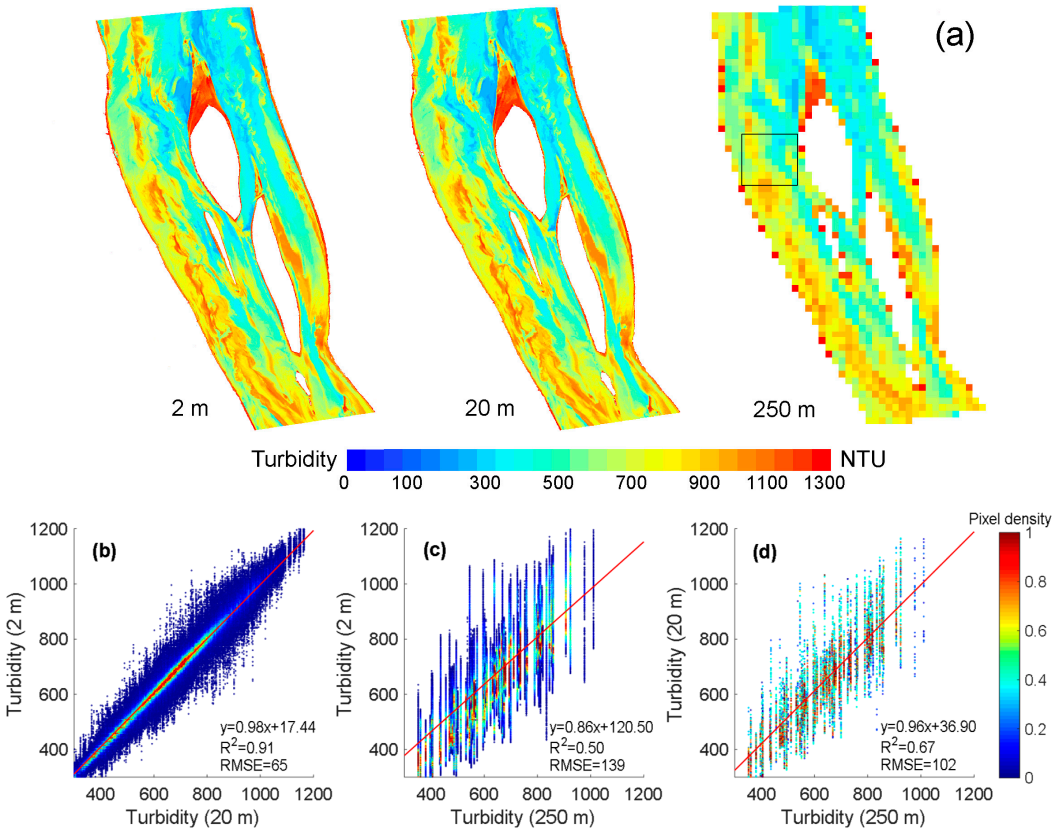

Figure 14. Comparison between Pléiades turbidity in Nephelometric Turbidity Unit (NTU) (24 May 2017) resampled to different spatial resolutions: (**a**) maps at 2, 20 and 250 m, and scatter plots comparing (**b**) 2 and 20 m, (**c**) 2 m and 250 m, (**d**) 20 m and 250 m turbidity values. The black square shows the area of interest considered in the scatter plots and the color bar denotes pixel density.

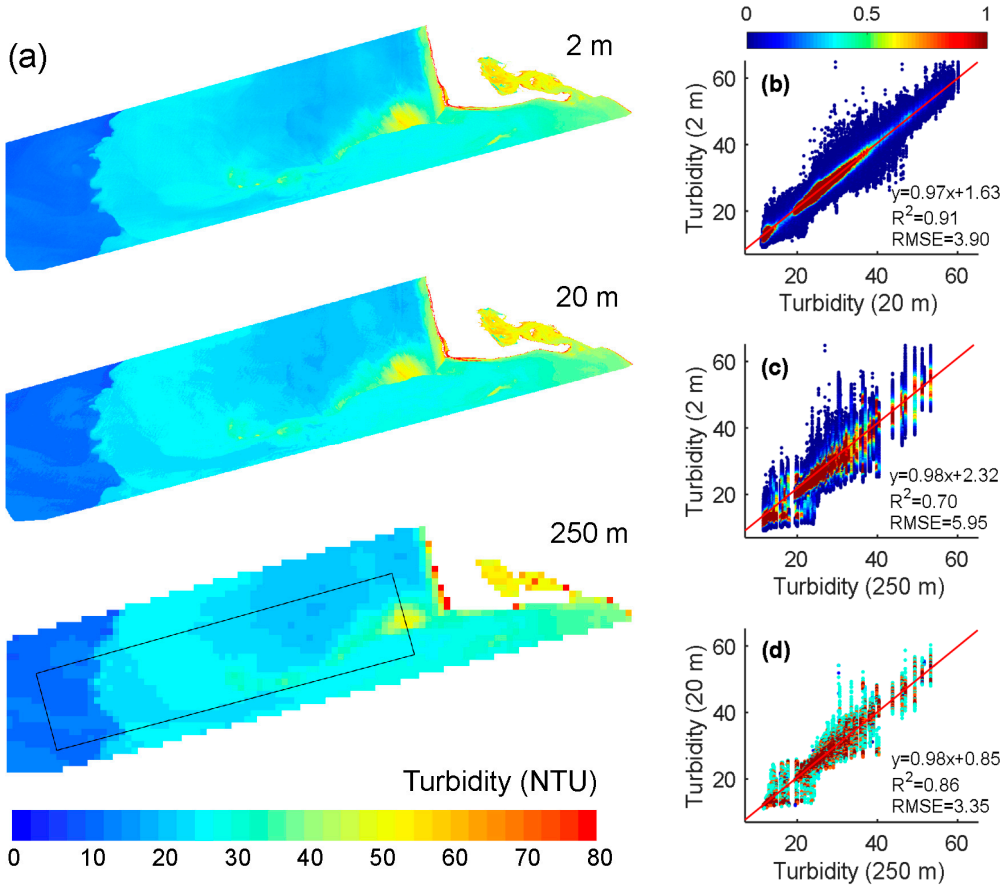

Figure 15. Comparison between Pléiades turbidity in Nephelometric Turbidity Unit (NTU) (7 April 2017) resampled to different spatial resolutions: (**a**) maps at 2, 20 and 250 m, and scatter plots comparing (**b**) 2 and 20 m, (**c**) 2 m and 250 m, (**d**) 20 m and 250 m turbidity values. The black square shows the area of interest considered in the scatter plots and the color bar denotes pixel density.

At the estuary mouth (site 2), the turbidity maps at 2, 20 and 250 m show a similar turbidity features (Figure 15). The observed differences in turbidity are 10% and 16% respectively for the 20 and 250 m products compared to 2 m. The difference between 250 m and 20 m is 9%. In this test site, the improvement from 20 m to 250 m is not as obvious as in test site 1.

The resampling shows that 20-m imagery shows good agreement with the 2-m imagery in both sites: MAPE 8–10% with R^2 of 0.91 (Figures 14b and 15b). The agreement between the 250 and 2 m products is worse, especially for site 1, with R^2 of 0.50 and intercept of 120.5 NTU (Figure 14c). These results indicate that 250 m imagery would underestimate peak values, and overestimate the low values, especially in variable and highly turbid sites. The performance of the 250 m product in test site 2 is better, with an R^2 of 0.70 and an intercept of 2.32 NTU (Figure 15c).

4. Discussion

4.1. About Validation

The results presented here show that water reflectance in the green, red and NIR bands as function of turbidity can be retrieved accurately from Pléiades imagery (Figure 5) in site 1. In site 2, the green and red reflectances compare well between OLI and Pléiades. The comparison between the MODIS and Pléiades products is not as good, especially in the green band. This worse performance can be explained by

(i) the time differences between the images: 2 hour 25 minutes between MODIS/Aqua and 45 minutes between MODIS/Terra and Pléiades, and 1 hour 40 minutes between MODIS/Aqua and Terra.

In the macro-tidal Gironde Estuary, such time differences induce significant turbidity variations [20,21]. When comparing MODIS/Terra and MODIS/Aqua satellite products (same sensor and atmospheric correction), differences consistent with those from Pléiades are observed (Figure 7a,b). The advection of water masses and sinking of suspended particles between two image acquisitions explain a significant part of the observed differences. Changes in the atmosphere may also occur during this time difference. The good agreement between Pléiades and OLI products is likely caused by the short time difference (22 minutes) between the satellite data acquisitions.

(ii) the different spatial resolutions of the three sensors result in different sensitivity to fine turbidity features (e.g. fronts), especially for the MODIS green band at 500 m, (iii) the different spectral responses of the sensors, and the applied corrections including radiometric calibration and atmospheric correction methods result in inevitable differences between the Pléiades, OLI and MODIS products.

Red and NIR band reflectances are used to derive turbidity products from Pléiades imagery. The turbidity for test site 1 corresponds well with autonomous in situ measurements for a wide range of turbidity (Figure 8b). The DSF atmospheric correction hence is appropriate for the retrieval of turbidity in the turbid and extremely turbid waters of the GE, similar to previous results obtained in coastal and estuarine waters [33,46].

4.2. Advantages of Metre-Scale Pléiades Data in Monitoring Water Quality Parameters

The advantages of Pléiades data, compared to SPOT-like (20 m) and MODIS-like (250 m), in monitoring water quality parameters in a dynamic water zone, over the whole estuary, and in small or confined areas are discussed below.

Along representative transects in test site 1 and test site 2 (Figures 12 and 13), both the 2 m and 20 m spatial resolution data show detailed variations of turbidity while the 250 m resolution introduces a loss of information, especially for test site 1. The very high spatial resolution of Pléiades shows much better results than the resampled 250 m product in test site 1, indicating the usefulness of this kind of imagery in maximum turbidity zones and zones with sharp turbidity variations. For test site 2, smaller differences are observed between 2 m, 20 m and 250 m resolution images (Figure 13). The benefit of having metre-scale satellite observations is less evident in the mouth area.

For the mapping of turbidity in large sections of the GE (Figures 14 and 15), an improvement is also observed using higher resolution satellite data. However, the improvement of spatial resolution from 20 m to 2 m (differences of turbidity $\leq 10\%$) is not as significant as from 250 m to 2 m (differences $\leq 18\%$). Therefore, over a large water body, even in a macro-tidal estuary which is a highly dynamic and turbid water zone, the advantage of metre-scale Pléiades satellite data is actually limited.

At smaller scale, around the Pauillac turbidity station located by the shores of the estuary, coarser spatial resolutions than Pléiades data result in an overestimation (8.27% for the 20 m and 26% for the 250 m resolution) of turbidity based on comparisons with in situ measurements. This is caused by the contamination of pixels due to sharp turbidity variations and mixed pixels in the near shore area. Hence, high-spatial-resolution imagery is required for retrieving the small-scale turbidity variations in such areas (Figure 11). Pléiades data can also be used to detect the turbulent phenomena of the Gironde Estuary such as the strong turbidity variations over test site 1. Human activities or constructions can be observed sharply with 2 m resolution Pléiades images, such as ship and airplane tracks, but also dredging plumes. The water turbidity can also be mapped inside ports (e.g., Figure 11), which certainly can help in the management of sediment transport and deposits in the estuary, thus help the management of the dredging activities conducted daily to prevent the filling of ports and navigation channels. Such detailed information can hardly be provided by other sensors associated to a coarser spatial resolution. In the Appendix A, twelve Pléiades images are shown to illustrate metre-scale and short-term variability of water turbidity in the GE (Figures A1 and A2).

4.3. Dataset and Methodology Limitations

The 2012 and 2013 SeaSWIR dataset (field turbidity and water hyperspectral reflectance measurements) was used in this study to obtain relationships between water turbidity and water reflectance in the Green, Red and NIR spectral bands of satellite sensors, with ρ values ($\rho = Rrs^{*}\pi$, dimensionless) ranging from 0.09 to 0.19, 0.09 to 0.22 and 0.01 to 0.15, respectively, in the Green, Red and NIR bands, and turbidity values ranging from 57.9 to 1484.7 NTU.

This dataset covers well the ranges observed in the Pléiades satellite data in test site 1 (central part of the estuary: the most turbid waters) but has some limitations in test site 2 (the less turbid waters of the mouth area) where turbidity values typically range from ~3 to ~100 NTU [21]. The turbidity retrieval algorithm was therefore mainly designed for test site 1 in the present study, which certainly explains the very satisfactory results obtained in terms of validation in this area (Figure 8b, Table 4). Such validation could not be performed in test site 2. In the near future, additional in situ measurements of water reflectance and turbidity will be carried out in the mouth area (test site 2) where a new MAGEST station (located in Le Verdon) is about to provide continuous turbidity field data notably for the calibration of algorithms and validation of satellite products.

The differences between Pléiades-1A and Pléiades-1B radiometric specifications was not taken into account in the present study, but these sensors have quite similar Relative Spectral Responses at Blue, Green, Red and NIR wavebands (Figure 3), resulting in very limited differences (MAPE of 0.9%, 1.6% and 3%, respectively, for the Green, Red and NIR bands) in terms of simulated water reflectances, based on the SeaSWIR dataset.

5. Conclusions

Very high-spatial-resolution (2 m) Pléiades satellite data was used for the first time to retrieve the water reflectance and turbidity in a macro-tidal estuary (the Gironde). The Dark Spectrum Fitting (DSF) atmospheric correction algorithm (Vanhellemont and Ruddick, 2018) was validated in several steps, showing that accurate reflectances can be retrieved from Pléiades over moderately to highly turbid estuarine waters. Turbidity values derived from Pléiades data showed a very good agreement with in situ data recorded by the shore of the estuary (Pauillac station), with MAPE of 10%. A full atmospheric correction is recommended for turbidity monitoring in the Gironde Estuary, as lower errors are retrieved compared to in situ data for the DSF-corrected (10%) than either for the Rayleigh-corrected (40%) or top-of-atmosphere reflectance (57%).

Pléiades data were spatially averaged to 20 m and 250 m pixel sizes to simulate the spatial resolutions of high (SPOT, MSI, OLI) and medium (MODIS, OLCI) satellite sensors. The results showed that Pléiades imagery provides higher detail and a more accurate retrieval of turbidity at the Pauillac autonomous monitoring station. The 20 m and 250 m pixels were contaminated by the shallow muddy waters and non-water pixels, and systematically resulted in an overestimation of field-measured turbidity. The spatial variations of water turbidity at 2, 20 and 250 m were compared along representative transects and for subsets of the images. Results showed limited differences between 2 m and 20 m satellite products, with MAPE $\leq$ 10%. The difference between 250 m and 2 m data was found to be larger, especially at test site 1, with MAPE $\leq$ 18%.

The improvement of spatial resolution from 250 m and 20 m to 2 m provides better estimates of water turbidity based on matchups between satellite-derived data and field measurements. Moreover, the 2 m resolution allows for the accurate mapping of turbidity inside ports and around pontoons, and detecting the release of sediments by dredging ships in the estuary. In the future, small-scale features, such as dredging plumes, could be studied for retrieving more specific information such as particle size and/or composition) by using very high-resolution Pléiades images.

Author Contributions: Conceptualization, D.D. and Y.L.; Software, Q.V.; Validation, Y.L.; Formal analysis, Y.L.; Resources, D.D.; Data curation, Q.V.; Writing—original draft preparation, Y.L.; Writing—review and editing, D.D. and Q.V.; Supervision, D.D. All authors have read and agreed to the published version of the manuscript.

Funding: This research was funded by the Federal Belgian Science Policy Office (BELSPO) under the STEREO III Programme PONDER project (SR/00/325) and supported by program for scientific research start-up funds of Guangdong Ocean University (R19124).

Acknowledgments: The authors wish to thank the many organizations for proving data used in this analysis, including the NASA, USGS, SeaSWIR project and MAGEST network. The MAGEST network is financially supported by the following organizations: AEAG (Agence de l'Eau Adour-Garonne); SMIDDEST (Syndicat MIxte pour le Développement Durable de l'ESTuaire de la Gironde); SMEAG (Syndicat Mixte d'Etudes et d'Aménagement de la Garonne); EPIDOR (Etablissement Public Interdépartemental de la Dordogne); EDF; GPMB (Grand Port Maritime de Bordeaux); Conseil Régional Aquitaine; CG-33 (Conseil Général de Gironde); Ifremer; CNRS; Université Bordeaux 1. Four anonymous reviewers are thanked for their feedback which greatly improved the structure of this manuscript.

Conflicts of Interest: The authors declare no conflict of interest.

Appendix A. Water Turbidity Mapping

In this Appendix, twelve Pléiades images are shown to illustrate small-scale and short-term variability of water turbidity in the GE (Figures A1 and A2). The images show water turbidity vary by a factor 10 in the Gironde MTZ area (test site 1) and that turbidity was systematically lower in the river mouth (test site 2). The turbidity in both sites correlates well to the tidal conditions in Paulliac and Cordouan as shown in Table 2.

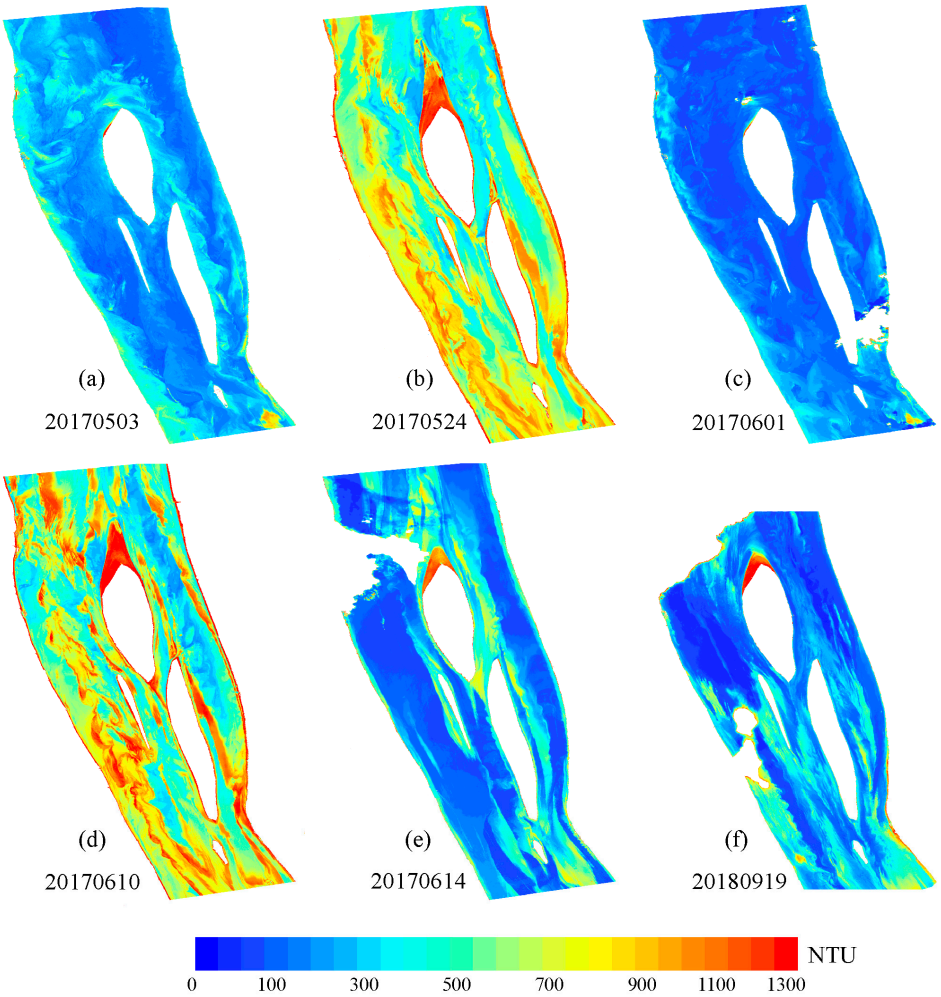

Figure A1. Water turbidity mapping with Pléiades images in test site 1. Land and cloud were masked. A type of turbulent 'helicoidal' current is observed in (**b**,**d**).

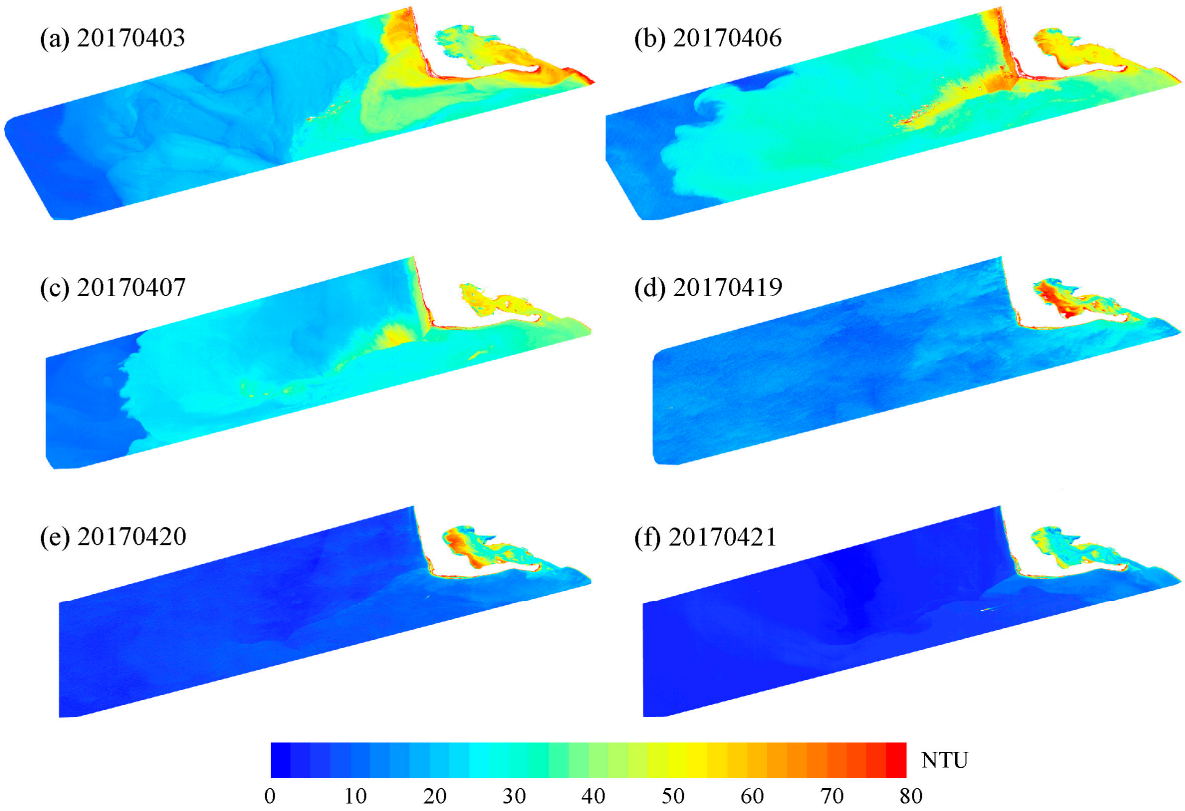

Figure A2. Water turbidity mapping with Pléiades images in test site 2. Land and cloud were masked. Turbidity fronts can be observed in (**a**–**c**).

References

1. Barnes, B.B.; Hu, C.; Kovach, C.; Silverstein, R.N. Sediment plumes induced by the Port of Miami dredging: Analysis and interpretation using Landsat and MODIS data. *Remote Sens. Environ.* **2015**, *170*, 328–339. [CrossRef]
2. Jay, S.; Guillaume, M. A novel maximum likelihood based method for mapping depth and water quality from hyperspectral remote-sensing data. *Remote Sens. Environ.* **2014**, *147*, 121–132. [CrossRef]
3. Olmanson, L.G.; Brezonik, P.L.; Bauer, M.E. Airborne hyperspectral remote sensing to assess spatial distribution of water quality characteristics in large rivers: The Mississippi river and its tributaries in minnesota. *Remote Sens. Environ.* **2013**, *130*, 254–265. [CrossRef]
4. Doxaran, D.; Devred, E.; Babin, M. A 50% increase in the mass of terrestrial particles delivered by the Mackenzie River into the Beaufort Sea (Canadian Arctic Ocean) over the last 10 years. *Biogeosciences* **2015**, *12*, 3551–3565. [CrossRef]
5. Ozbay, G.; Fan, C.; Yang, Z. Relationship between land use and water quality and its assessment using hyperspectral remote sensing in mid-atlantic estuaries. In *Water Quality*; IntechOpen: Rijeka, Croatia, 2017.
6. Ritchie, J.C.; Cooper, C.M. Remote sensing techniques for determining water quality: Applications to TMDLs. In Proceedings of the TMDL Science Issues Conference, Water Environment Federation, Alexandria, VA, USA, 4–7 March 2001; pp. 367–374.
7. Shang, S.; Lee, Z.; Shi, L.; Lin, G.; Wei, G.; Li, X. Changes in water clarity of the Bohai Sea: Observations from MODIS. *Remote Sens. Environ.* **2016**, *186*, 22–31. [CrossRef]
8. Giardino, C.; Bresciani, M.; Cazzaniga, I.; Schenk, K.; Rieger, P.; Braga, F.; Matta, E.; Brando, V. Evaluation of multi-resolution satellite sensors for assessing water quality and bottom depth of Lake Garda. *Sensors* **2014**, *14*, 24116–24131. [CrossRef]
9. Vanhellemont, Q.; Neukermans, G.; Ruddick, K. Synergy between polar-orbiting and geostationary sensors: Remote sensing of the ocean at high spatial and high temporal resolution. *Remote Sens. Environ.* **2014**, *146*, 49–62. [CrossRef]

10. Vanhellemont, Q. Automated water surface temperature retrieval from Landsat 8/TIRS. *Remote Sens. Environ.* **2020**, *237*, 111518. [CrossRef]
11. Vanhellemont, Q.; Ruddick, K. Turbid wakes associated with offshore wind turbines observed with Landsat 8. *Remote Sens. Environ.* **2014**, *145*, 105–115. [CrossRef]
12. Qiu, Z.; Xiao, C.; Perrie, W.; Sun, D.; Wang, S.; Shen, H.; Yang, D.; He, Y. Using Landsat 8 data to estimate suspended particulate matter in the Yellow River estuary. *J. Geophys. Res. Oceans* **2017**, *122*, 276–290. [CrossRef]
13. Constantin, S.; Doxaran, D.; Constantinescu, Ș. Estimation of water turbidity and analysis of its spatio-temporal variability in the Danube River plume (Black Sea) using MODIS satellite data. *Cont. Shelf Res.* **2016**, *112*, 14–30. [CrossRef]
14. Constantin, S.; Constantinescu, Ș.; Doxaran, D. Long-term analysis of turbidity patterns in Danube Delta coastal area based on MODIS satellite data. *J. Mar. Syst.* **2017**, *170*, 10–21. [CrossRef]
15. Zhang, Y.; Shi, K.; Zhou, Y.; Liu, X.; Qin, B. Monitoring the river plume induced by heavy rainfall events in large, shallow, Lake Taihu using MODIS 250 m imagery. *Remote Sens. Environ.* **2016**, *173*, 109–121. [CrossRef]
16. Doxaran, D.; Froidefond, J.-M.; Lavender, S.; Castaing, P. Spectral signature of highly turbid waters: Application with SPOT data to quantify suspended particulate matter concentrations. *Remote Sens. Environ.* **2002**, *81*, 149–161. [CrossRef]
17. Doxaran, D.; Castaing, P.; Lavender, S. Monitoring the maximum turbidity zone and detecting fine-scale turbidity features in the Gironde estuary using high spatial resolution satellite sensor (SPOT HRV, Landsat ETM+) data. *Int. J. Remote Sens.* **2006**, *27*, 2303–2321. [CrossRef]
18. Gernez, P.; Lafon, V.; Lerouxel, A.; Curti, C.; Lubac, B.; Cerisier, S.; Barillé, L. Toward Sentinel-2 high resolution remote sensing of suspended particulate matter in very turbid waters: SPOT4 (Take5) Experiment in the Loire and Gironde Estuaries. *Remote Sens.* **2015**, *7*, 9507–9528. [CrossRef]
19. Novoa, S.; Doxaran, D.; Ody, A.; Vanhellemont, Q.; Lafon, V.; Lubac, B.; Gernez, P. Atmospheric corrections and multi-conditional algorithm for multi-sensor remote sensing of suspended particulate matter in low-to-high turbidity levels coastal waters. *Remote Sens.* **2017**, *9*, 61. [CrossRef]
20. Doxaran, D.; Froidefond, J.-M.; Castaing, P.; Babin, M. Dynamics of the turbidity maximum zone in a macrotidal estuary (the Gironde, France): Observations from field and MODIS satellite data. *Estuar. Coast. Shelf Sci.* **2009**, *81*, 321–332. [CrossRef]
21. Constantin, S.; Doxaran, D.; Derkacheva, A.; Novoa, S.; Lavigne, H. Multi-temporal dynamics of suspended particulate matter in a macro-tidal river Plume (the Gironde) as observed by satellite data. *Estuar. Coast. Shelf Sci.* **2018**, *202*, 172–184. [CrossRef]
22. Li, J.; Chen, X.; Tian, L.; Huang, J.; Feng, L. Improved capabilities of the Chinese high-resolution remote sensing satellite GF-1 for monitoring suspended particulate matter (SPM) in inland waters: Radiometric and spatial considerations. *ISPRS J. Photogramm. Remote Sens.* **2015**, *106*, 145–156. [CrossRef]
23. Shang, P.; Shen, F. Atmospheric correction of satellite GF-1/WFV imagery and quantitative estimation of suspended particulate matter in the Yangtze estuary. *Sensors* **2016**, *16*, 1997. [CrossRef] [PubMed]
24. Liu, H.; Li, Q.; Shi, T.; Hu, S.; Wu, G.; Zhou, Q. Application of sentinel 2 MSI images to retrieve suspended particulate matter concentrations in Poyang Lake. *Remote Sens.* **2017**, *9*, 761. [CrossRef]
25. Pahlevan, N.; Sarkar, S.; Franz, B.; Balasubramanian, S.; He, J. Sentinel-2 Multispectral Instrument (MSI) data processing for aquatic science applications: Demonstrations and validations. *Remote Sens. Environ.* **2017**, *201*, 47–56. [CrossRef]
26. Caballero, I.; Stumpf, R.P.; Meredith, A. Preliminary Assessment of Turbidity and Chlorophyll Impact on Bathymetry Derived from Sentinel-2A and Sentinel-3A Satellites in South Florida. *Remote Sens.* **2019**, *11*, 645. [CrossRef]
27. Sawaya, K.E.; Olmanson, L.G.; Heinert, N.J.; Brezonik, P.L.; Bauer, M.E. Extending satellite remote sensing to local scales: Land and water resource monitoring using high-resolution imagery. *Remote Sens. Environ.* **2003**, *88*, 144–156. [CrossRef]
28. Ekercin, S. Water quality retrievals from high resolution IKONOS multispectral imagery: A case study in Istanbul, Turkey. *Water Air Soil Pollut.* **2007**, *183*, 239–251. [CrossRef]
29. Liu, J.; Zhang, Y.; Yuan, D.; Song, X. Empirical estimation of total nitrogen and total phosphorus concentration of urban water bodies in China using high resolution IKONOS multispectral imagery. *Water* **2015**, *7*, 6551–6573. [CrossRef]

30. Dorji, P.; Fearns, P. Impact of the spatial resolution of satellite remote sensing sensors in the quantification of total suspended sediment concentration: A case study in turbid waters of Northern Western Australia. *PLoS ONE* **2017**, *12*, e0175042. [CrossRef]
31. Fichot, C.G.; Downing, B.D.; Bergamaschi, B.A.; Windham-Myers, L.; Marvin-DiPasquale, M.; Thompson, D.R.; Gierach, M.M. High-resolution remote sensing of water quality in the San Francisco Bay–Delta Estuary. *Environ. Sci. Technol.* **2016**, *50*, 573–583. [CrossRef]
32. ASTRIUM. *PLEIADES Imagery User Guide*; An EADS Company, 2012. Available online: https://www.cscrs.itu.edu.tr/assets/downloads/PleiadesUserGuide.pdf (accessed on 3 March 2020).
33. Vanhellemont, Q.; Ruddick, K. Atmospheric correction of metre-scale optical satellite data for inland and coastal water applications. *Remote Sens. Environ.* **2018**, *216*, 586–597. [CrossRef]
34. Vanhellemont, Q. Daily metre-scale mapping of water turbidity using CubeSat imagery. *Opt. Express* **2019**, *27*, A1372–A1399. [CrossRef] [PubMed]
35. Vermote, E.; Tanré, D.; Deuzé, J.; Herman, M.; Morcrette, J.; Kotchenova, S. Second Simulation of a Satellite Signal in the Solar Spectrum-Vector (6SV). 6S User Guide Version. 2006, Volume 3, pp. 1–55. Available online: http://6s.ltdri.org/files/tutorial/6S_Manual_Part_1.pdf (accessed on 3 March 2020).
36. Kotchenova, S.Y.; Vermote, E.F.; Matarrese, R.; Klemm, F.J. Validation of a vector version of the 6S radiative transfer code for atmospheric correction of satellite data. Part I: Path radiance. *Appl. Opt.* **2006**, *45*, 6762–6774. [CrossRef]
37. Feldman, G.C.; McClain, C.R. *l2gen, Ocean Color SeaDAS*; NASA Goddard Space Flight Center: Greenbelt, MD, USA, 2010. Available online: https://oceancolor.gsfc.nasa.gov/docs/format/l2oc_modis/ (accessed on 3 March 2020).
38. Wang, M.; Wei, S. The NIR-SWIR combined atmospheric correction approach for MODIS ocean color data processing. *Opt. Express* **2007**, *15*, 15722–15733. [CrossRef] [PubMed]
39. Vanhellemont, Q.; Ruddick, K. Advantages of high quality SWIR bands for ocean colour processing: Examples from Landsat-8. *Remote Sens. Environ.* **2015**, *161*, 89–106. [CrossRef]
40. Etcheber, H.; Schmidt, S.; Sottolichio, A.; Maneux, E.; Chabaux, G.; Escalier, J.M.; Wennekes, H.; Derriennic, H.; Schmeltz, M.; Quéméner, L.; et al. Monitoring water quality in estuarine environments: Lessons from the MAGEST monitoring program in the Gironde fluvial-estuarine system. *Hydrol. Earth Syst. Sci.* **2011**, *15*, 831–840. [CrossRef]
41. Schmidt, S.; Etcheber, H.; Sottolichio, A.; Castaing, P. Le reseau MAGEST: Bilan de 10 ans de suivi haute-fréquence de la qualité des eaux de l'estuaire de la Gironde. *Mesures Haute Résolution Dans L'environnement Marin Côtier*; Schmitt, F.G., Lefevre, A., Eds.; Presses du CNRS, 2016; pp. 51–60. Available online: http://www.magest.u-bordeaux1.fr/files/docs/PublicationHFMAREL2014-SchmidtS.pdf (accessed on 3 March 2020).
42. Knaeps, E.; Ruddick, K.G.; Doxaran, D.; Dogliotti, A.I.; Nechad, B.; Raymaekers, D.; Sterckx, S. A SWIR based algorithm to retrieve total suspended matter in extremely turbid waters. *Remote Sens. Environ.* **2015**, *168*, 66–79. [CrossRef]
43. Knaeps, E.; Doxaran, D.; Dogliotti, A.; Nechad, B.; Ruddick, K.; Raymaekers, D.; Sterckx, S. The SeaSWIR dataset. *Earth Syst. Sci. Data* **2018**, *10*, 1439–1449. [CrossRef]
44. Luo, Y.; Doxaran, D.; Ruddick, K.; Shen, F.; Gentili, B.; Yan, L.; Huang, H. Saturation of water reflectance in extremely turbid media based on field measurements, satellite data and bio-optical modelling. *Opt. Express* **2018**, *26*, 10435–10451. [CrossRef]
45. Nechad, B.; Ruddick, K.; Park, Y. Calibration and validation of a generic multisensor algorithm for mapping of total suspended matter in turbid waters. *Remote Sens. Environ.* **2010**, *114*, 854–866. [CrossRef]
46. Vanhellemont, Q. Adaptation of the dark spectrum fitting atmospheric correction for aquatic applications of the Landsat and Sentinel-2 archives. *Remote Sens. Environ.* **2019**, *225*, 175–192. [CrossRef]